An Atomic Force Microscopy Tip Model for Investigating the Mechanical Properties of Materials at the Nanoscale

Michele Alderighi[1], Vincenzo Ierardi[1], Maria Allegrini[2], Francesco Fuso[2], and Roberto Solaro[1, *]

[1]*Department of Chemistry and Industrial Chemistry, University of Pisa, via Risorgimento 35, 56126 Pisa, Italy*
[2]*Department of Physics, CNISM and INFM/CNR-PolyLab, University of Pisa, Largo B. Pontecorvo 3, 56127 Pisa, Italy*

Investigation of the mechanical properties of materials at the nanoscale is often performed by atomic force microscopy nanoindentation. However, substrates with large surface roughness and heterogeneity demand careful data analysis. This requirement is even more stringent when surface indentations with a typical depth of a few nanometers are produced to test material hardness. Accordingly, we developed a geometrical model of the nanoindenter, which was first validated by measurements on a reference gold sample. Then we used this technique to investigate the mechanical properties of a coating layer made of Balinit C, a commercially available alloy with superior anti-wear features deposited on steel. The reported results support the feasibility of reliable hardness measurements with truly nanosized indents.

Keywords: AFM, Nanoindentation, Nanomechanics, Hardness, Balinit C.

At local scale, material properties such as, hardness and elastic modulus often differ from those acquired by conventional measurements.[1–4] Still, precise knowledge of those parameters is frequently required both to reliably assess the material properties and to design new applications. Nanonindentation testing, also known as depth sensing indentation (DSI),[5] is a popular technique to address similar issues. Likewise in traditional indentation tests, a controlled load is applied to the sample surface by a nanosized indenter. In macroscopic experiments the size of the mark left by the indenter is evaluated by optical imaging. On the other hand, in DSI the displacement of the indenter probe is recorded when a known load is first applied and then removed. Material hardness H can then be directly related to the maximum applied load P_{MAX}, according to

$$H = P_{MAX}/A_C \qquad (1)$$

where the indented area A_C can be evaluated by geometrical considerations. Neglecting higher orders in the approximation, the area can be expressed as a function of the final indentation depth h_F:

$$A_C \propto C_{tip} h_F^m \qquad (2)$$

where the C_{tip} factor takes into account the indenter shape. The coefficient m also depends on the actual indenter geometry. This approach, based on the work by Oliver and Pharr[6] and on the original calculations by Sneddon,[7] enabled investigations entailing loads as small as tenths of microNewton and depths as small as a few nanometers.[8] Indeed, dislocation starvations created in such small regions can lead to hardening effects resulting in increased hardness for indentation depths in the tens of nanometers range.[9] Description of the involved microscopic processes is often cumbersome because of the simultaneous occurrence of many phenomena. Instrumental size effects associated with the used experimental methods must be also carefully accounted for. As a result, the issue whether instrumental factors or material properties dominate is still debated.

When dealing with rough surfaces or inherently heterogeneous blends and alloys, the lack of surface imaging can prevent reliable reconstruction of the sample properties by DSI. The possibility to precisely identify the region to indent is often desirable in order to reconstruct the local variations of material properties. Atomic force microscopy (AFM) offers a straightforward method to combine imaging and indentation. Relatively large loads can be applied at predefined locations by using stiff cantilevers and hard tips. Switching to imaging mode allows for mapping the surface morphology before and after the indentation, thus gaining an invaluable insight into sample properties.

Several materials were already analyzed by AFM-based nanoindentation.[10–15] However, a few issues must be carefully addressed in order to make quantitative evaluation of hardness and elastic modulus, essentially aimed at distinguishing between intrinsic and extrinsic size effects.[16] Indeed, conventional tests afford different

COMMUNICATION

hardness values (e.g., Vickers, Knoop) depending upon the indenter geometry. When using AFM, the indenter shape is constrained by the choice of the tip, which is typically assumed to be pyramidal. However, the actual shape of the tip end is very important and it must be carefully considered. For instance, the effect of blunt tips has been demonstrated;[4] recently it has been pointed out that the transition from spherical to pyramidal shape can strongly affect data interpretation.[17]

The choice of the AFM probe is crucial for carrying out hardness measurement. Stiff cantilevers offer the advantage of rather large loads even for small displacement, thus opening the door to nanosized material indentations. The tip material is also important. Because of the relatively high hardness of the investigated samples, diamond tips must be used to prevent tip deformation that could mask the sample behavior. Rather sharp tip are also needed to carry out reliable AFM imaging. We used DNISP probes (Veeco Instruments), which are made of a single diamond crystal with the shape of an equilateral triangular pyramid, directly glued to a stainless steel cantilever (elastic constant 224 N/m). The angle α is 47° and the cantilever is held at a tilt angle $\theta = 12°$ in the microscope head. Calibration of the vertical displacement sensitivity was regularly carried out by using a hard Al_2O_3 substrate. A commercial AFM (Multimode with Nanoscope IV controller, Veeco Instruments) equipped with a PicoForce stage allowing for closed-loop scans in the Z direction (J-type scanner) was used in nanoindentation experiments. Piezo displacement (both vertical and lateral) and cantilever deflection were collected also by a digital oscilloscope connected to the signal access module in order to have an additional time-resolved check of the instrumental behavior.

Interpretation of nanoindentation data requires knowledge of the dependence of the intender projected area on the indentation depth. The projected area of a tilted pyramid is $A_{tilt} = (L'h')/2$ (Fig. 1). This can be found by defining the pyramid edge as $a = x/\cos(\alpha + \theta)$ and the tilted indentation depth as $x' = x/\cos(\theta)$. The tilted projection of the edge over the tilted base is $b = a \sin(\alpha)$. The heights

of the triangle and of the tilted triangle (the base of the tip) are $h = 3b/2$ and $h' = h \cos(\theta)$, respectively; the sides of the base and of the tilted base are $L = 3^{1/2}b$ and $L' = ((L/2)^2 + h'^2)^{1/2}$, respectively.

The projected area A_{tilt} can be evaluated from these geometrical quantities, which, in turn, are directly related to the indentation depth h. In other words, C_{tip} and m in Eq. 2 can be evaluated by setting $A_{tilt} = A_C$. However, this model is inaccurate. Indeed, the tip apex cannot be considered truly point-like, but a rounded end must be taken into account. This is confirmed by the image of a TGT1 spike reference grid (NT-MDT) recorded in non-contact mode. Since the grid topographical features are much smaller than the typical tip size (the nominal curvature radius of the grating spikes is less than 10 nm), the resulting image reproduces essentially the inverted shape of the tip. Image analysis confirmed a spherical shape with radius $R = 80$ nm; this value, which can depend also on the aging of the tip, was constantly monitored by imaging the spike grid before and after each nanoindentation run.

Accordingly, the indenter is (mostly) spherical when the penetration depth is below a certain threshold, whereas a pyramidal shape is predominant at larger indentation values. The intermediate regime is obviously critical since indentation depths in the tens of nanometers are particularly relevant to assess the material behavior at the nanoscale. Our geometrical model considers a smooth transition from the spherical to the pyramidal shape, obtained by assuming parallel surfaces in the transition region. The relationship giving the effective radius R_{eff} to be used in data interpretation as a function of R is

$$R_{eff} = R(1 - \sin(\alpha)) \qquad (3)$$

In our case, the transition takes place at $R_{eff} = 21.5$ nm. The projected area of a spherical indenter depends on the indentation depth h according to

$$A_{sphere} = 2\pi R h_F - \pi h^2 \qquad (4)$$

leading to a power coefficient m completely different from the pyramidal case.

Combination of the tilted pyramid behavior with that of a spherical shape gives the plot shown in Figure 1, where a slope change clearly occurs close to the R_{eff} value. This behavior can explain the findings of Ref. [17], that is a slope change of the hardness versus indentation depth curve. Accounting for instrumental size effects is thus mandatory in order to retrieve reliable information.

This model was validated by using a gold film deposited on silicon (Veeco Instruments) as reference substrate. The plastic behavior of gold has been extensively studied and simulated also at the nanoscale;[18] published macroscopic analysis data suggest $H = 1.4$–1.5 GPa. An array of indentation marks corresponding to different indentation loads and depths was produced on the gold surface. For each indentation, the force versus displacement curve
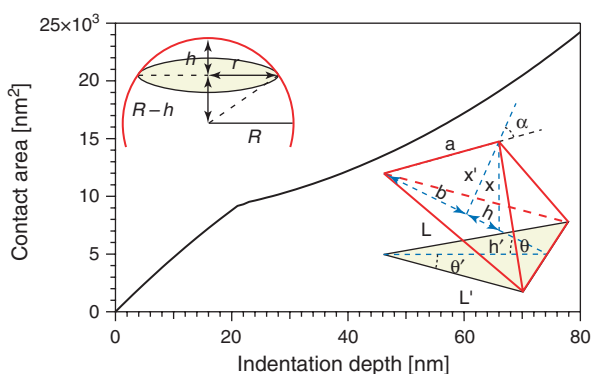
Fig. 1. Contact area versus indentation depth curve, computed by our geometrical model. In the insets: sketches of the spherical and pyramidal geometries relevant to the model.
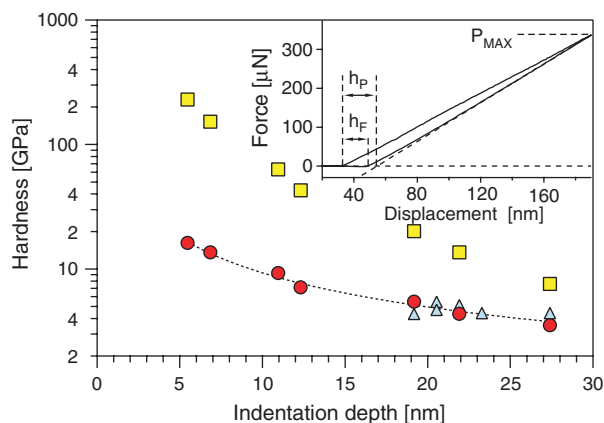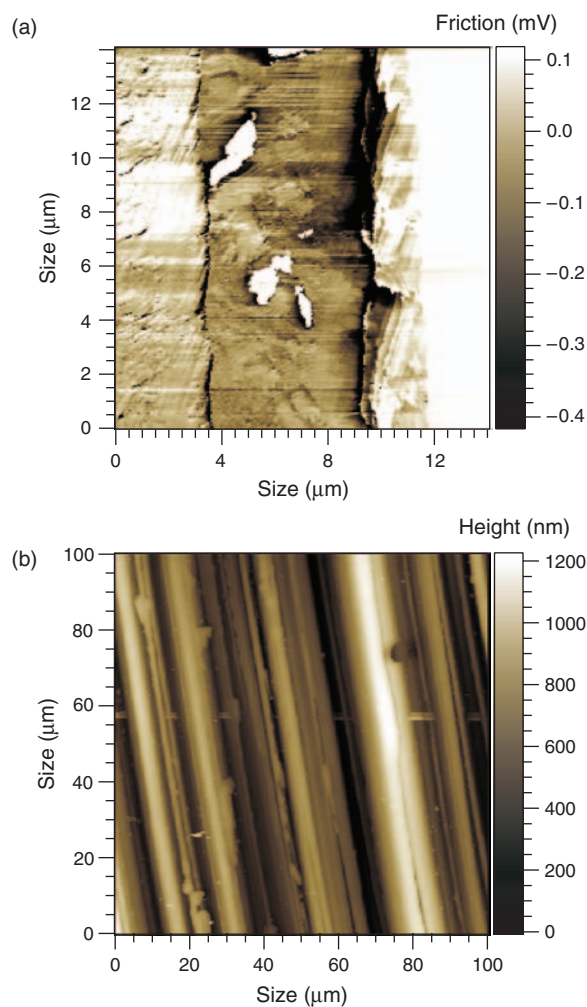
Fig. 2. Hardness versus indentation depth h_F calculated for a gold sample from force versus piezo displacement curves according to: our tip model assuming either h_F (circles) or h_P (triangles) as the indentation depth; a pure pyramidal tip shape (squares, for clarity hardness has been divided by two). The dashed line represents a power-like behavior with $H_0 = 1.8$ GPa and $\mu = -1.2$. In the inset: typical force versus piezo displacement curve.

was acquired by using the instrument software. A typical curve is shown in the inset of Figure 2. All indentations were performed by setting a constant vertical displacement speed of 200 nm/s and no time delay at the maximum applied load. Material mechanical properties in fact depend on the strain rate and duration.[4] By monitoring the lateral deflection of the cantilever, we get rid of effects related to the torsional motion of the cantilever/tip assembly, selecting data with purely vertical deflection contributions. Measurements were obviously affected by some uncertainty associated also with the low signal level when small loads are applied. By acquiring a large set of data, we estimated an overall relative instrumental uncertainty below 20%. Since measurements can be affected by a large variety of stray and spurious phenomena, as, e.g., sample shifts, mechanical noise, locally enhanced adhesion phenomena due to impurities, we continuously monitored the elastic behavior of the sample by analyzing the slope of the unloading curve.[5] In all measurements, the elastic modulus of the material was constant and in good agreement with reference data.
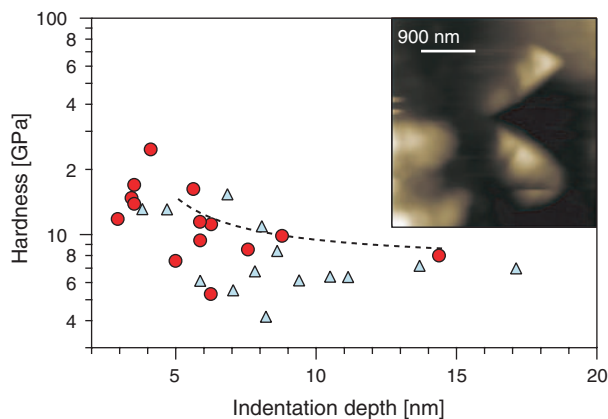
Force versus displacement curves allow for direct evaluation of the final indentation depth h_F, defined as the distance between the loading curve start and the unloading curve end (Fig. 2). The plastic depth h_P, evaluated as the intersection of the tangent to the unloading curve with the zero load line,[5] has to be considered when plastic surfaces are indented. Both h_F and h_P were used to determine the contact area A_C according to our model. Once evaluated A_C, we derived the corresponding hardness by Eq. (1). Measurements were especially addressed to investigate the sample behavior at indentation depths close to R_{eff}. Figure 2 presents the results obtained by using either h_F or h_P together with data evaluated by assuming a simple tilted pyramidal shape for the tip. As expected,

a wrong large hardness was attained in the latter case because of a strongly underestimated contact area. On the contrary, our geometrical model led to a rather good agreement with reference data. More specifically, we achieved a slightly decreasing hardness at increasing penetration depth by identifying the indentation depth as h_F. A best fit to a power law function ($H = H_0 + h^\mu$) gave an asymptotic value $H_0 = 1.5 \pm 0.1$ GPa with a power exponent $\mu \sim -0.3$. This effect can be attributed to the occurrence of intrinsic size effects.[16] By analyzing the same data as a function of the plastic depth h_P, the hardness was about 4 GPa almost independently of the indentation depth. In other words, any size effect practically disappears, suggesting that contact area is actually underestimated in the regime of small tip penetration if plastic recovery of the surface is neglected. On the other hand, the agreement with reference data gets worse suggesting that extrapolation of the indentation depth from the slope of the unloading curve is no longer applicable for small or very small indented volumes.[5]

To test the validity of our model, we analyzed the plastic deformation of Balinit C,[19] a wear-protection layer

Fig. 3. AFM friction map of a cross section of Balinit C coated steel (a) and top view AFM topography of the same sample (b).

Fig. 4. Hardness versus indentation depth for a Balinit C layer calculated from force versus piezo displacement curves according to: our tip model assuming either h_F (circles) or h_P (triangles) as the indentation depth. The dashed line represents a power-like behavior with $H_0 = 6.6$ GPa and $\mu = -1.2$. In the inset: non-contact AFM topography of the indentation mark left on the sample surface after application of a maximum load $P_{MAX} > 150$ μN.

deposited on steel, by AFM to evaluate its mechanical properties at the nanoscale. Contrarily to most literature reports, Balinit C has poor surface homogeneity and remarkable roughness. The investigated samples consisted of Balinit C-coated steel cut into square specimens (10×10 mm^2). Balinit C is a commercially available WC/C (α-C:H:W) coating alloy with superior performance in terms of wear protection for heavy duty applications.[20] The Balinit layer is about 6 μm thick as shown by the AFM friction map of the sample cross-section (Fig. 3(a)). Besides debris following cross-section preparation, the image suggests the occurrence of a rather compact coating layer at the micrometer scale. Comparison of the average friction level of the Balinit layer (middle band) with that of the steel substrate (left band) indicates a smaller friction coefficient for the coating, in line with product specifications.[19] The material surface is rather rough (Fig. 3(b)), mostly as a consequence of mechanical polishing. Surface roughness is about 690 nm over a 100×100 μm^2 area. The inhomogeneous composition and morphology make Balinit C a typical example of systems where nanomechanical analysis represents a challenging task.

Results acquired on the Balinit coating are summarized in Figure 4. The inset shows the indentation mark left on the sample surface after application of a load $P_{MAX} > 100$ μN. Hardness values are rather scattered, very likely because of the poor material homogeneity. The hardness of the Balinit layer is clearly larger than that of gold. Due to the different plastic behavior of these materials, the computed Balinit hardness does not depend much on the use of either h_F or h_P. More specifically, the use of h_F leads to $H_0 = 5.5 \pm 1.0$ GPa with a power coefficient

$\mu = -1.0$. The dependence on h_P is less pronounced and the H average value is about 7 GPa. Reference data are not available for the hardness of Balinit at the nanometer scale. Material specifications[19] indicate a macroscopic Knoop parameter HK $\sim$ 1000–1500 depending on test conditions. Although HK to hardness conversion is not straightforward, the Knoop value roughly corresponds to $H \sim 7$–8 GPa, in fair agreement with our findings.

In conclusion, the developed model highlights the role of the actual indenter shape (the AFM tip, in our case). In particular, the transition between pyramidal and spherical geometries is of paramount importance. This model leads to reliable hardness measurements also at indentation depths of a few nanometers and when data interpretation is made difficult by the poor material homogeneity at the local scale.

References and Notes

1. J. D. Kiely, R. Q. Hwang, and J. E. Houston, *Phys. Rev. Lett.* 81, 4424 (**1998**).
2. M. Goken, M. Kempf, and W. D. Nix, *Acta Mater.* 49, 903 (**2001**).
3. D.-L. Liu, T.-M. Lu, G.-C. Wang, and R. C. Picu, *Appl. Phys. Lett.* 85, 3053 (**2004**).
4. F. Wang, P. Huang, and K. W. Xu, *Appl. Phys. Lett.* 90, 161921 (**2007**).
5. M. F. Doerner and W. D. Nix, *J. Mater. Res.* 1, 601 (**1986**).
6. W. C. Oliver and G. M. Pharr, *J. Mater. Res.* 7, 1564 (**1992**).
7. I. N. Sneddon, *Int. J. Engng. Sci.* 3, 47 (**1965**).
8. B. Bhushan, Nanotribology and Nanomechanics: An Introduction, Springer, New York (**2005**).
9. W. D. Nix, J. R. Greer, G. Feng, and E. T. Lilleodden, *Thin Solid Films* 515, 3152 (**2007**), and references therein.
10. D. Drechsler, A. Karbach, and H. Fuchs, *Acta Mater.* 47, 1043 (**1999**).
11. M. Kempf, M. Goken, and H. Vehoff, *Appl. Phys. A* 66, S843 (**1998**).
12. S. A. S. Asif, K. J. Wahl, and R. J. Colton, *J. Mater. Res.* 15, 546 (**2000**).
13. S. E. Grillo, M. Ducarroir, M. Nadal, E. Tournic, and J. P. Faurie, *J. Phys. D* 36, L5 (**2003**).
14. S. Garcia-Manyes, A. G. Guell, P. Gorositza, and F. Sanz, *J. Chem. Phys.* 123, 114711 (**2005**).
15. T. Scholz, K. K. McLaughlin, F. Giuliani, W. J. Clegg, F. J. Espinoza-Beltran, M. V. Swain, and F. A. Schneider, *Appl. Phys. Lett.* 91, 62903 (**2007**).
16. Y. Huang, F. Zhang, K. C. Hwang, W. D. Nix, G. M. Pharr, and G. Feng, *J. Mech. Phys. Solids* 54, 1668 (**2006**).
17. W. Chen, M. Li, T. Zhang, Y.-T. Cheng, and C.-M. Cheng, *Mat. Sci. Eng. A* 445, 323 (**2007**).
18. D. Lee, X. Wei, M. Zhao, X. Chen, S. C. Jun, J. Hone, and J. W. Kysar, *Modelling Simul. Materi. Sci. Eng.* 15, S181 (**2007**), and references therein.
19. Balinit is a Registered Mark by Oerlikon Balzers (see http://www.oerlikon.com).
20. F. J. Teeter and M. Berger, *Gear Technol.* 13, 27 (**1996**).